International Journal of QUANTUM CHEMISTRY

Density Functional Theory Study of the Reactivity and Electronic Structure of the Transesterification of Triacetin in Biodiesel Production via a Sulfated Zirconia Heterogeneous Catalysis

Jesús Muñiz,*[a,b] Roger Castillo,[b] José B. Robles,[b] and Enrique Sansores[c]

This DFT study examined the interaction of a sulfated zirconia (SZ) slab model system (heterogeneous catalyst) and triacetin (a precursor in biodiesel production) using explicit methanol solvent molecules. Full geometry optimizations of the systems were performed at the B3LYP level of theory. Gibbs free energies provide insight into the spontaneity of the reactions along a three-step reaction mechanism for the transesterification of triacetin. Charge decomposition analysis revealed electronic charge transfer between the metallic oxide and the organic moieties involved in the reaction mechanism. Fukui indices indicate the likely locations on the SZ surface where catalysis may occur. The quadratic synchronous transit scheme was used to locate transition structures for each step of the transesterification process. The results are in agreement with the strongly acidic catalytic character of zirconium observed experimentally in the production of biodiesel. © 2016 Wiley Periodicals, Inc.

DOI: 10.1002/qua.25116

Introduction

Because of the excessive use of fossil fuels, which increase environmental pollution and consequently magnify the greenhouse effect, the search for alternative environmentally friendly fuels from effective renewable sources is of great relevance. In particular, the conversion of vegetable oils, such as those from *Jatropha curcas*,[1] canola,[2] palm,[3] palm kernel,[4] coconut,[5] sunflower,[6] and feedstock, such as recycled fried oils, into biodiesel represents a reliable and sustainable choice for the production of biofuels. In effect, the above feedstock is generated from triglycerides and free fatty acids. There are several advantages[7,8] that make biodiesel synthesis a profitable alternative to fuel production; indeed, biodiesel can be used in a mixture with conventional diesel fuel with adequate performance and no engine modifications. Furthermore, biodiesel provides a better combustion because of the presence of oxygen, it reduces toxicity to the environment, it is biodegradable, and it reduces the greenhouse effect because of a closed CO cycle and reduces dependence on petroleum-based diesel fuels. Additionally, biodiesel requires natural renewable resources whose production stimulates the development of rural economies.

Triglycerides, the organic species that include vegetable oils and animal fats, are composed of esters of glycerol with three chains of aliphatic or olefinic free fatty acids with 12–24 carbon atoms. The production of biodiesel is usually performed through transesterification. In this case, triglycerides react with a low-molecular-weight alcohol, often in the presence of a homogeneous catalyst, to produce a mixture of fatty acid alkyl esters, commonly termed biodiesel, and glycerol. In this respect, triglycerides must be converted to simple esters to have specific flow features and combustion properties that are useful in conventional diesel engines. Biodiesel may be readily obtained from several methodologies, such as base-catalyzed transesterification,[9] acid-catalyzed transesterification,[10] enzyme-catalyzed transesterification,[11] hydrolysis, pyrolysis,[12] and supercritical alcohol transesterification.[13] Homogeneous catalysis is the most widely implemented technique, with the use of KOH or NaOH as the catalyst, whereas methanol or ethanol is used as the alcohol because of their low cost and availability.[14] Despite the high conversion rates for such transesterification processes, the price of biodiesel obtained from homogeneous catalysis is not as competitive as that of commercial diesel because the catalyst is completely consumed in the production process. A high-quality feedstock, such as virgin or refined vegetable oil, is then required because of the presence of water and free fatty acids, which eliminate side effects such as hydrolysis or saponification. Thus, it is clear that a heterogeneous catalysis, in which a solid

[a] *J. Muñiz*
Instituto de Energías Renovables, Universidad Nacional Autónoma de México, Priv. Xochicalco s/n, Col. Centro, Temixco, Morelos, CP 62580, México. Fax: (+52) 555 622 9741
E-mail: jms@ier.unam.mx

[b] *J. Muñiz, R. Castillo, J. B. Robles*
Cuerpo Académico de Energía y Sustentabilidad, Universidad Politécnica de Chiapas, Carretera Tuxtla-Villaflores km 1 + 500, Suchiapa, Chiapas, CP 29150, México

[c] *E. Sansores*
Instituto de Investigaciones en Materiales, Universidad Nacional Autónoma de México, Apartado Postal 70-360, México, DF, 04510, México

Contract grant sponsor: Consejo Nacional de Ciencia y Tecnología (CONACYT-México); contract grant number: 156591 (SEP-Ciencia Básica).
Contract grant sponsor: CONACYT Research Fellow-Universidad Nacional Autónoma de México; Cátedras-CONACYT (Project No. 1191).

catalyst is reused in the production process, would significantly decrease the production costs.[1] Moreover, transesterification and esterification processes may be achieved using this technique. In particular, the use of transition metal oxides as the heterogeneous catalyst, such as zirconium oxide, has attracted attention for biodiesel production because of their acidic properties.[1] Zirconia has been implemented in a variety of reactions, such as the alkylation of isobutene[15] and the isomerization of *n*-butane,[16] and its high activity has been correlated with its acidity. As a solid catalyst in transesterification processes, the acidity of zirconia is enhanced when its surface contains anions, such as sulfate and tungstate.[1] A comparative study between zirconium oxide and zinc oxide as solid catalysts in the transesterification of palm kernel oil at supercritical methanol showed that methyl ester yields were 64.5% for zirconium oxide and 86.1% for zinc oxide after 1 h of reaction time using 3 wt % catalyst and a 6:1 molar ratio of alcohol/oil. The process changed dramatically (with yields up to 90.3%) when sulfated zirconia (SZ) was used, which may be attributed to the high acidic strength of the sulfate anions on the SZ surface. Relatedly, the catalytic activities of ZrO_2/SO_4^{2-} and ZrO_2/WO_3^{2-} in the transesterification of triacetin were compared.[17] In this case, it was found that the specific surface areas and active site concentrations dominate the catalytic activity. Additionally, the calcination temperatures on the catalytic properties of ZrO/WO^{2-} for the transesterification of triacetin[18] were examined, and it was shown that the catalyst was active for transesterification and esterification reactions, despite relatively long reaction times. Other studies by Ramu et al.[19] reported that the acidity, which is correlated to the catalytic activity, decreased as the amount of WO increased because of excess coverage of WO on ZrO. Furuta et al.[20] studied the conversion of soybean oil over tungstated zirconia and found that the catalyst activity remained stable up to 100 h of use, demonstrating that zirconium catalysts possess a high reliability for transesterification processes. The use of SZ as an acid catalyst yields a higher triacetin conversion (57%) over other acid catalysts, such as WS, zeolite Hb, ETS-10(H), and Nafion.[17] Furthermore, SZ has the advantage that it is more robust, can withstand higher temperatures, and can participate in transesterification reactions as efficiently as sulfuric acid.

The recent syntheses of the heterogeneous catalysts Na-doped cubic ZrO_2[21] and sodium zirconate[22] have been reported, and it was shown that these new materials possess optimal properties for use in biodiesel transesterification reactions, with yields of 93 and 98.3%, respectively.

It has been found[17] that the transesterification of triglycerides occurs in three separate processes such that the free fatty acids interact with the alcohol to give a fatty acid alkyl ester, diglyceride, and monoglyceride as intermediates and then the final glycerol byproduct. Additionally, it has been demonstrated theoretically[23] and experimentally[17] that triglyceride may be successfully modeled with a smaller molecule, such as triacetin, as it possesses the same chemical functionality. It is important to note that this approximation may overestimate some interactions because of the lack of the long alkyl chains present in triglycerides, which may introduce steric and hydrophobic repulsions with respect to the heterogeneous catalyst. In this regard, the latter mechanism may proceed as depicted in Scheme 1, where the three-step reaction requires one mole of triacetin and three moles of methanol to give three moles of a linear ester and one mole of glycerol.

Theoretical studies on homogenous transesterification are very limited. To clarify the existence of tetrahedral intermediates along the reaction pathways of base-catalyzed transesterification, Tapanes et al.[24] performed an experimental and theoretical study on biodiesel formation from *Jatropha curcas* oil. The reaction pathways of monoglyceride were examined using the semiempirical AM1 model. A tetrahedral intermediate was found, and its dissolution was found to be the rate-determining step. The formation of the intermediate was attributed to the difference between the kinetics of methanolysis and ethanolysis and the alkoxide formation step. Hori et al.[25] reported a mechanism of the gas-phase acid-catalyzed hydrolysis of methyl acetate in the gas phase and in solution, modeled by both explicit and implicit solvent molecules. It was found that the reaction occurs once an explicit solvent molecule is included because solvent molecules enhance the nucleophilicity of the attacking water molecule, which is a weaker nucleophile than the hydroxide ion and permits cleavage of the —OCH group of acetic acid involved in the reaction. It was found that cleaving the —OCH group with a water-assisted proton transfer is the rate-determining step. Relatedly, Fox et al.[26] found that methanol was not able to bond to the carbonyl carbon to form an intermediate structure because of the lack of explicit solvent molecules. A DFT/B3LYP study[23] was performed on the thermodynamic and kinetic aspects of the methanolysis and hydrolysis reactions of triacetin. A mechanism involving an acid-catalyzed methanolysis reaction was proposed. Furthermore, the central carbon atom of glycerol was found to be quite reactive, which is consistent with observations based on NMR data. In these studies, triglyceride requires a reaction with the ester carbonyl moiety for the transesterification to proceed. In addition, a reaction mechanism involving the alkaline-catalyzed transesterification of pentylic acid triglyceride was studied using DFT/B3LYP.[27,28] It was shown that the activation energies are in good agreement with those determined experimentally. Nevertheless, a theoretical study of an acid-based heterogeneous catalysis for biodiesel production has not yet been explored. For this reason, the aim of this work is to provide insight into the reaction mechanisms of transesterification processes using an SZ model system as an acid heterogeneous catalyst.

Computational Methods

Geometry optimizations were performed at the DFT/B3LYP level of theory,[29] which combines exact Hartree-Fock exchange with the Lee, Yang, and Parr correlation functional. The search of transition-state structures was performed using the quadratic synchronous transit (QST3) scheme.[30,31] In this method, the quadratic region of the transition state is approached, and then an eigenvalue-following algorithm is

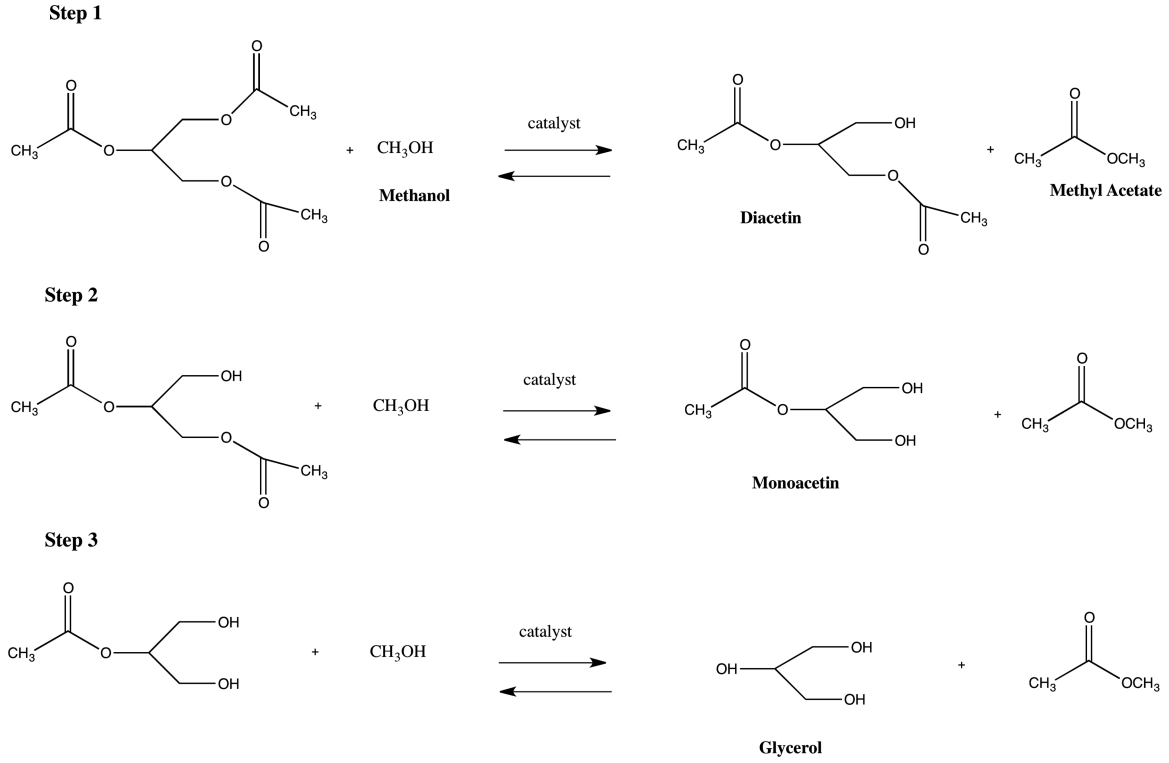

Scheme 1. Three-step reaction of triacetin transesterification involved in biodiesel production. Note that the overall reactions evolve in the presence of a heterogeneous catalyst.

used to complete the optimization procedure. The QST3 method is intended to find the transition structure by using an empirical estimate of the Hessian,[30,31] with structures for the reactant, product, and a guess for the transition state used as input. Finally, the scheme finds a state with an imaginary frequency that may be assigned to the transition structure. The Stuttgart small-core pseudo relativistic effective core potential ECP28MDF[32] with 12 valence electrons was used for Zr atoms with the optimized basis set[33] cc-pVTZ-PP. The 6-31++G(2df,p) basis set[34,35] was used for all non-Zr atoms.

In addition, charge decomposition analysis (CDA) calculations[36] were performed on the systems in this study. This analysis describes donor–acceptor interactions and partitions the molecular complex into two fragments. The method constructs the wave function of the complex in terms of a linear combination of donor and acceptor fragment orbitals. CDA returns the following contributions: charge donation from the occupied orbitals of the donor to the unoccupied orbitals of the acceptor, back-donation from the occupied orbitals of the acceptor to the unoccupied orbitals of the donor, and the repulsive polarization, which accounts for the charge removed from the overlapping area of the occupied orbitals of the donor and acceptor fragments. A correlation energy diagram was constructed at the scalar zero-order relativistic approximation (ZORA) including spin-orbit effects.[37,38] A Slater-type, high-quality triple-ζ plus one polarization basis set was used for this analysis.

Regarding the search for probable reactive sites in the metal clusters, Fukui local functions[39,40] for the electrophilic and nucleophilic moieties were evaluated via finite difference using NBO[41] gross natural charges (q). The equations behind the calculation of the Fukui and local softness indices were used to compare the reactivity properties among the different chemical species; these are presented in the Supporting Information. Additionally, an approach proposed by Chatarraj et al.[42] to account for local electrophilicity is given. All calculations were performed using the Gaussian 09 software package.[43] The ZORA calculations were performed with the Amsterdam Density Functional software package version 2013.01.[44]

Results and Discussion

Structural description and reactivity

SZ represents a reliable metal catalyst when it is used with organic moieties.[45,46] To study the catalytic properties of SZ, we considered an SZ model system that is based on previous calculations.[47–49] Experimental evidence suggests that SZ has a sulfated tetragonal ZrO_2 pyrosulfate surface structure, which can activate *n*-butane through an oxidative dehydrogenation step.[45] In the current case, and to the best of our knowledge, no experimental evidence on the surface structure of SZ for the transesterification of triacetin has been reported. It has been shown that the periodic structure of ZrO_2 may be computationally modeled using monoclinic, tetragonal, or cubic geometries.[48] The monoclinic configuration has been adopted in this work as a first attempt to model the catalytic properties

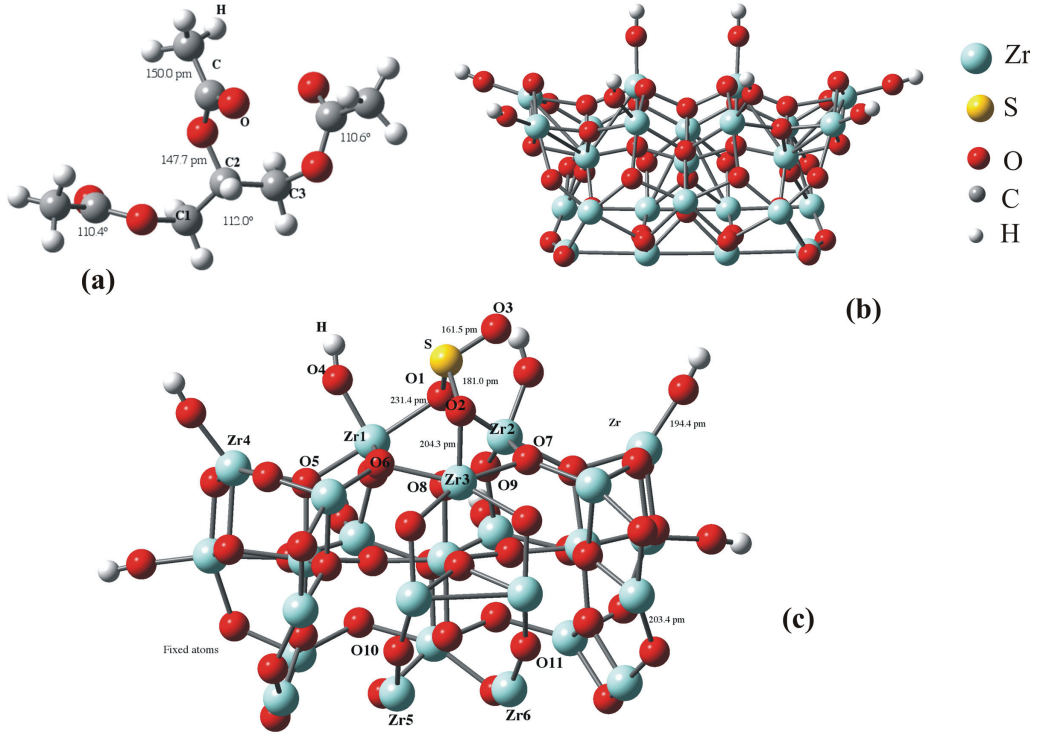

Figure 1. a) Structural description of triacetin. Main structural parameters (bond lengths and angles) are depicted for clarity. b) Ground-state geometry of zirconia. c) Ground-state geometry of sulfated zirconia. Main structural parameters (bond lengths and angles) are also depicted. The first three layers in the slab were kept fixed as no contributions from the deepest Zr atoms in the model are expected.

of SZ because this geometry is the only stable structure at room temperature.[50] The structure undergoes a transition to tetragonal at ~1480 K and to cubic at ~2650 K. As experimental observation of transesterification processes has been reported on SZ at 60°C,[17] a study of the phenomena is more appropriate using the monoclinic configuration. It is important to note that the relative stability of the SZ surface structure is sensitive to the concentration of sulfur-containing species. In general, experiments suggest that SZ possesses the species H_2SO_4/H_2O and SO_3/H_2O on its surface. From the latter, the pyrosulfate phase [$S_2O_7^{2-}$, 2H+, and H_2O] and the proton-free [SO_3] phase are the surface structures that persist for a wide range of temperatures and partial pressures.[45] As the aim of this study is to describe the catalytic process of triacetin transesterification, we focused on the [SO_3] structure because it is the simplest, possible comparative model of an SZ surface structure. Still, a comparative study of the latter two stable configurations of SZ on the conversion of triacetin remains highly desirable. However, such a study is beyond the scope of this work.

To reduce computational time, periodic conditions of the zirconia structure were not considered in this work. Instead, a slab model based on the monoclinic ZrO_2 structure with point group $P2_1/c$ was used. The ZrO_2 slab system, $Zr_{25}O_{48}H_8$ (see Fig. 1b), was saturated with hydrogen atoms to satisfy valencies and was optimized at the level of theory described above. The atoms at the bottom of this slab (i.e., 17 Zr sites and 23 O sites) were kept fixed during the optimization procedure because no participation of these centers is expected for catalytic activity. A total of 45 atoms at the surface were allowed to relax during the optimization procedure. To model SZ, a second geometry optimization of the ZrO_2 system was performed that included a SO_3 molecule attached to its surface (see Fig. 1c). The main structural parameters of this optimized geometry are reported in Table 1. It is seen that the SO_3 molecule is tightly bound to the ZrO_2 surface. Such bonding may be considered to be covalent, where SO_3 is attached to the surface through Zr1—O1 and Zr2—O1 bonding (see Fig. 1c), with bond lengths of 231.4 pm and 230.1 pm, respectively, and through Zr3—O2, with a bond distance of 204.3 pm.

Our SZ model system, namely, $Zr_{25}SO_{51}H_8$, is intended to possess superior catalytic activity from that observed for pristine zirconia as a result of its acidic nature, as previously noted by Kanougi et al.[48] and others.[46,47,49] To investigate this notion more fully, molecular electrostatic potential (MEP) surfaces were determined (Fig. 2). As seen, the acidic nature of zirconia is modified as SO_3 interacts with the slab as an increased negative charge contribution is present at the zirconia surface where the SO_3 molecule is adsorbed. This indicates that the acidic character of SZ is reproduced with the current slab model.

Some other structures, such as H_2SO_4 adsorbed on ZrO_2, have also been studied.[48] In such systems, one or more oxygen atoms are attached to the ZrO_2 surface. In this regard, both cluster and periodic models have been used. In the former case, a catalytic active site is taken from the periodic structure, and its reactivity and surface properties are studied. For instance, Babou et al.[51] studied S—ZrO_2 by modeling the

Table 1. Main structural parameters of the SZ ground-state geometry.

No.	Bond	Bond length (pm)
Main bonding distances		
1	S—O1	181.0
2	S—O2	181.0
3	S—O3	161.5
4	Zr1—O1	231.4
5	Zr2—O1	230.1
6	Zr1—O4	193.8
7	Zr1—O5	212.5
8	Zr1—O6	217.9
9	Zr3—O2	204.3
9	Zr2—O7	215.9
10	Zr2—O9	205.1
11	Zr3—O6	224.7
12	Zr3—O7	225.7
13	Zr5—O10	200.4
14	Zr6—O11	200.6
Main bonding angles		
No.	Bond angle	Angle (°)
1	O1—S—O2	98.0
2	Zr1—O1—Zr2	105.1
3	O6—Zr3—O7	131.3
4	O5—Zr1—O1	112.7
5	O2—Zr2—O7	44.1
6	O4—Zr1—O6	110.2
7	Zr4—O5—Zr1	136.8

ZrO_2 (001) plane and considered a $Zr(OH)_4$ tetrahedron with two water molecules that interact with the Zr atom. It was found that sulfuric acid interacts through hydrogen bonding with two oxygen atoms on the ZrO_2 surface. Using this approach, Hong et al.[52] suggested a mechanism for the initiation process of the isomerization of butane over a small sulfated ZrO_2 model cluster. Periodic models have been used by Haase and Sauer[53] in their study of the interaction of sulfuric acid with the (101) and (001) surfaces of a ZrO_2 tetragonal phase.

In addition to the MEP analysis and considering that the adsorption of SO_3 on zirconia plays an important role in catalysis because of its enhanced acidic behavior, we compared the catalytic properties of zirconia with SZ. A standard procedure was implemented in which an NH_3 molecule was used as a probe to measure its adsorption energies on both surfaces. The adsorption of NH_3 on surfaces is used widely to compare the catalytic properties of systems and to determine the availability of adsorption sites. In the current case, the adsorption energies were estimated to be on the same order of magnitude. The SZ gives an adsorption energy that is 9 kcal/mol smaller than that of zirconia. Such a difference may be attributed to the change in charge density around the catalyst because of the presence of SO_3. Consequently, the charge distribution on the MEP surface is changed, as shown in Figure 2. Figure 2a depicts the distribution of the electrostatic charge density. As seen, an excess of positive charge on the surface of the zirconia catalyst and the model is present. This is consistent with previous experimental observations, which supports the view that zirconia is an acid catalyst.[48] When the zirconia catalyst adsorbs SO_3, the electrostatic potential distribution is altered and the locations of the excess positive charge becomes changed, which slightly reduces its acidic character; consequently, the adsorption energy of NH_3 decreases. Because the difference in adsorption energy is small, and because the SZ catalyst has been used experimentally, the SZ system was adopted as our model catalyst in the current study.

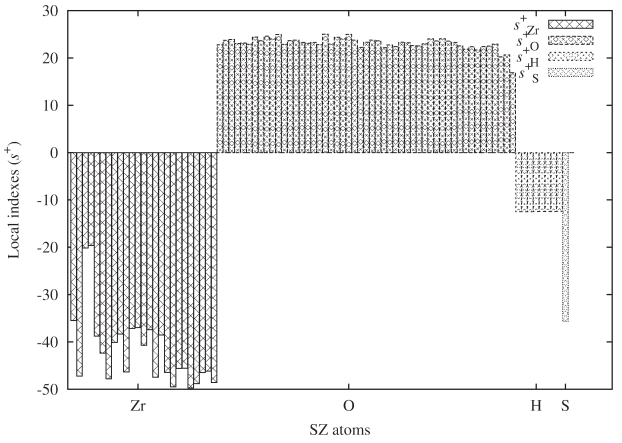

Figure 3. Fukui local indexes of nucleophilicity (s^+).

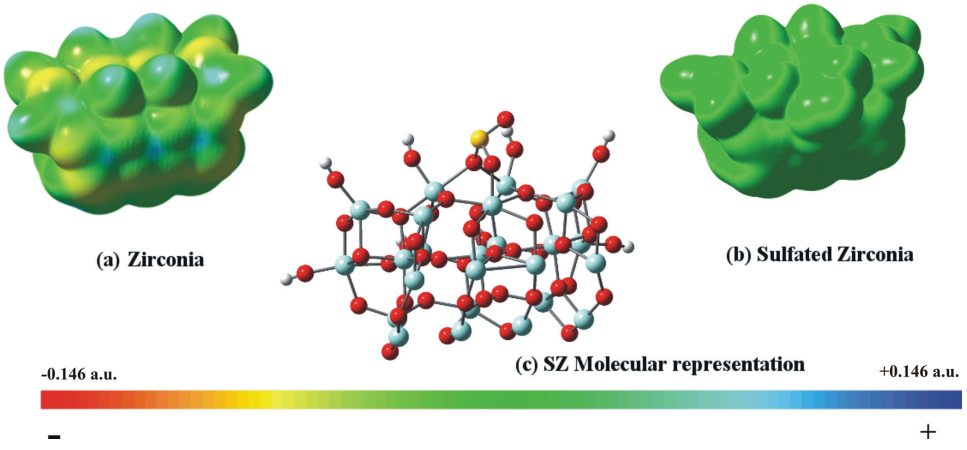

Figure 2. a) Molecular electrostatic potential (MEP) surface of the slab zirconia model. b) MEP surface of the sulfated zirconia system. c) SZ molecular representation in the same geometrical orientation of the former MEPs.

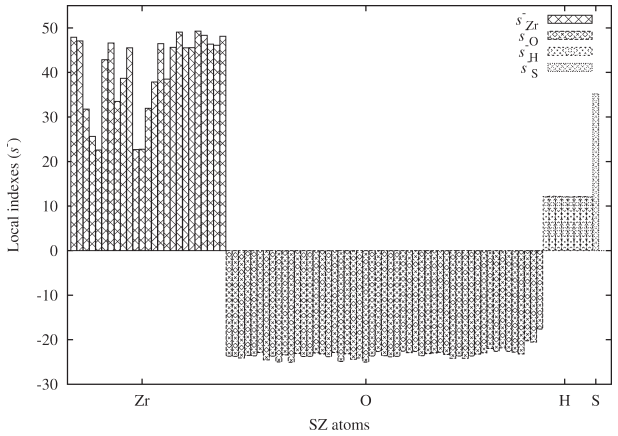

Figure 4. Fukui local indexes of electrophilicity (s^-).

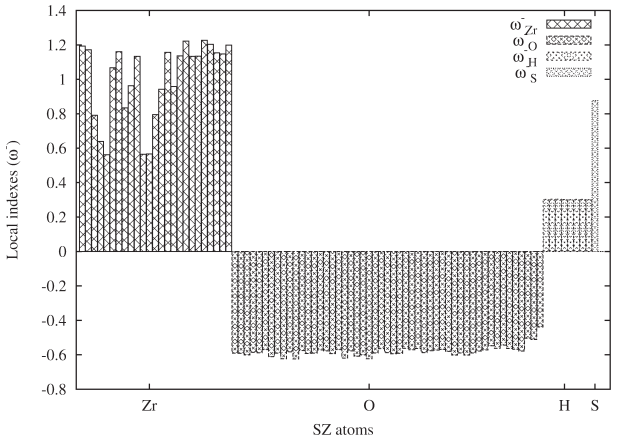

Figure 5. Generalized electrophilicity index of reactivity (ω^-). The indexes correspond to possible reactive sites around the SZ slab system centered at the corresponding atoms.

To have a more general criterion on the reactivity properties of the SZ system, we performed a Fukui index analysis because it has been found that this approach quantitatively describes susceptible sites on a molecular system when reactivity may be important.[42] Based on the SZ model, we calculated the electrophilic attack (f^-) and nucleophilic attack (f^+) Fukui indices using a finite-difference approximation, as described by Eqs. (1) and (2), respectively, given in the Supporting Information. The f^- and f^+ parameters provide insight into candidate sites in the system where reactivity may play a role. Fukui indices were computed using gross natural charges, as stated in the Supporting Information. Because it is desirable to compare reactivity properties among complexes, local softness (s) parameters were also computed from the equations given in the Supporting Information. These results are reported in Figures 3 and 4.

As depicted in Figure 4, the highest s^- local softness indices correspond to Zr atoms. In addition, the S center possesses a significant s^- index (s_S^-) relative to Zr, as indicated by the s_S^- value being only 13% smaller than the average s_{Zr}^- indices for the SZ slab model. In addition, the oxygen atoms possess significant s^+ values (see Fig. 3). The Zr sites and the S center possess the highest local softness indices among all of the atoms in the model. This indicates that reactivity may arise primarily at Zr, with an important contribution from S, which activates the surface. It is known[42] that the Fukui function is an intramolecular index and is not adequate to examine intermolecular reactivity. Thus, as stated in the Supporting Information, local indices of electrophilicity are more useful parameters than global indices because the former contain information of the latter, in addition to the site selectivity of the system toward electrophilic or nucleophilic attack. In this respect, because of differences of global electrophilicities of the two systems, the best reactive sites of the two distinct systems can only be understood in the framework of local philicity and not on Fukui functions. According to Figure 5, reactivity by electrophilic attack in our SZ slab model would be expected to occur at the Zr atoms and the S center because the highest reactivity descriptors ω^- are located at those atoms, namely, ω^-_{Zr} and ω^-_S, respectively. ω^-_{Zr} ranges from ~0.6 to 1.2, whereas the ω^-_S descriptor is 12.6% smaller than the average ω^-_{Zr} value. It may be inferred that an electrophilic attack is most probable at the Zr atoms, with a similar participation from the S site. Collectively, these contributions give rise to the overall catalytic activity observed in this model, which is consistent with experimental observations.[17] Moreover, as seen in Figure 6, it may be inferred that a nucleophilic attack is expected at the oxygen atoms because their ω^+ descriptors are the highest.

Reaction mechanism

We used the optimized SZ slab system as the catalyst in the transesterification process to model the three-step biodiesel reaction mechanism described in Scheme 1. In addition, we used triacetin to model the triglycerides involved in the reactions (see Fig. 1a) because this molecule preserves the electronic properties contained in long-chain triglycerides, as previously presented. It is known that the overall reaction of triacetin has six possible pathways including 12 elementary steps.[23] The experimental work of López et al.[17] suggests a possible route to achieve transesterification as a three-step

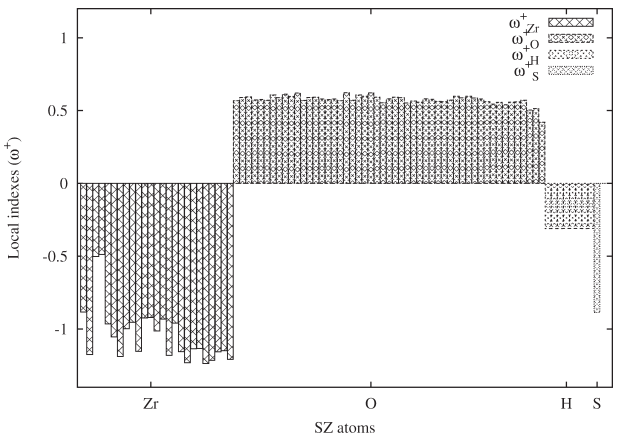

Figure 6. Generalized nucleophilicity index of reactivity (ω^+). The indexes correspond to possible reactive sites susceptible to nucleophilic attack around the SZ slab.

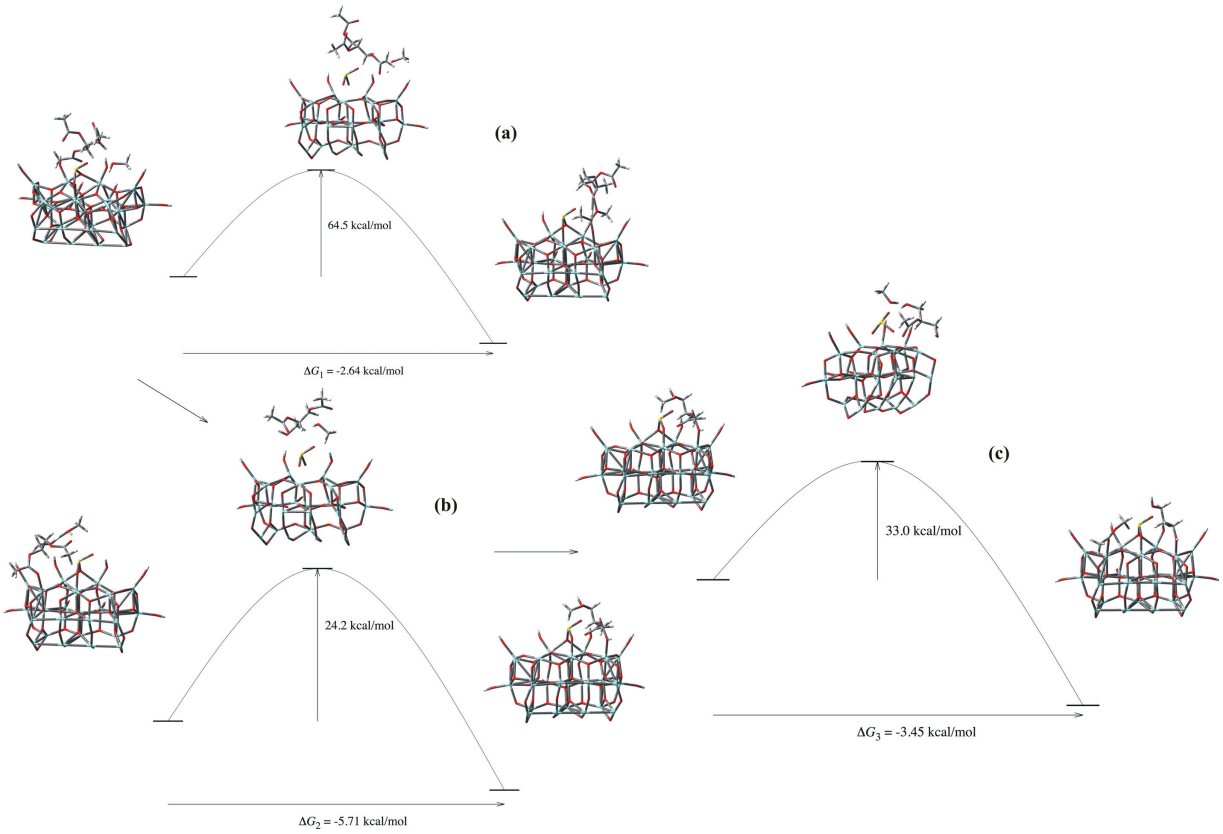

Figure 7. a) Reaction mechanism of triacetin (**T**) transesterification to diacetin (**D**) in the presence of methanol (**M**) with methyl acetate (**MA**) as byproduct. b) Reaction mechanism of **D** transesterification to monoacetin (**MO**) with **MA** as byproduct. c) Reaction mechanism of **MO** transesterification to glycerol (**G**) with **MA** as byproduct. Please note that a close-up of each of the processes involved in the overall reaction is also presented in Figure 8.

reaction to give biodiesel (Scheme 1). Taking the latter into consideration, we performed our calculations based on this assumption to generalize and compare our theoretical results with experiment. The full reaction coordinate is depicted in Figure 7. In the first step, triacetin interacts with the SZ catalyst in the presence of an alcohol (i.e., methanol) that acts as the solvent. We modeled the effect of this solvent with explicit methanol molecules for each step of the reaction. A full geometry optimization was performed to model this interaction. At this first step, all systems involved (i.e., triacetin, methanol, and the SZ model surface) were previously optimized at the level of theory described in the "Computational Methods" section. After geometry relaxation, the methanol molecule interacts directly with the —$OCOCH_3$ group of triacetin (see Figs. 1a and 8a), and this configuration is used to find the transition-state geometry TS1. The structural parameters of the SZ system remain virtually unchanged after relaxation (see Fig. 8). The angles of the relaxed structure of triacetin are altered by ~1%, especially the $(C1—C2—C3)_T$ angle, as shown in Figures 1a, 7a, and 8a. Triacetin is adsorbed on the SZ catalyst through weak hydrogen-type interactions, with bond distances of 370.0, 316.2, and 282 pm for $H1_T—H2_{SZ}$, $H3_{SZ}—H4_M$, and $H5_T—H6_M$, respectively. Methanol is found to retain its geometrical structure during adsorption, and a hydrogen-type interaction is observed at $H3_{SZ}—H4_M$.

As seen, the transition state (TS1) is also presented in the reaction coordinate of Figures 7a and 8a. The $O1_M—H4_M$ bond of methanol is completely broken and a hydrogen atom is released. This state has an energy barrier of 64.5 kcal/mol. The released hydrogen atom interacts with triacetin and is located at 114 pm from the closest oxygen atom. The intermolecular distance from the organic moiety to the SZ surface catalyst is 258 pm; the structural parameters of the surface are not significantly distorted. A structural representation of the products is depicted in Figure 7a, and a close-up view is given in Figure 8a. As expected, a diacetin moiety is formed with methyl acetate. This structure was also fully optimized with certain fixed coordinates, as described above. A clear interaction involving methyl acetate and the SZ surface is observed; indeed, a bonding distance of 217 pm is observed between the $O1_{MA}$ atom of methyl acetate and the $Zr1_{SZ}$ atom on the SZ surface (a close-up view is shown at P1 on Fig. 8a). The structural parameters around the periphery of $Zr1_{SZ}$ are distorted from those measured at the surface of the reactant's geometry, that is, bond distances around the $Zr1_{SZ}$ atom are elongated ~2% from those computed prior to the interaction. The computations show an analogous behavior along the full network, indicating that the role of the Zr atoms on the adsorption of methyl acetate cannot be neglected. The latter indicates that the surface catalyst aids in the process of transesterification, and the elongation of the bonding parameters in the periphery of the Zr atoms distorts the network at the metal surface to allow the methyl acetate to anchor onto the surface, giving rise to the formation of methyl acetate in the first step of the

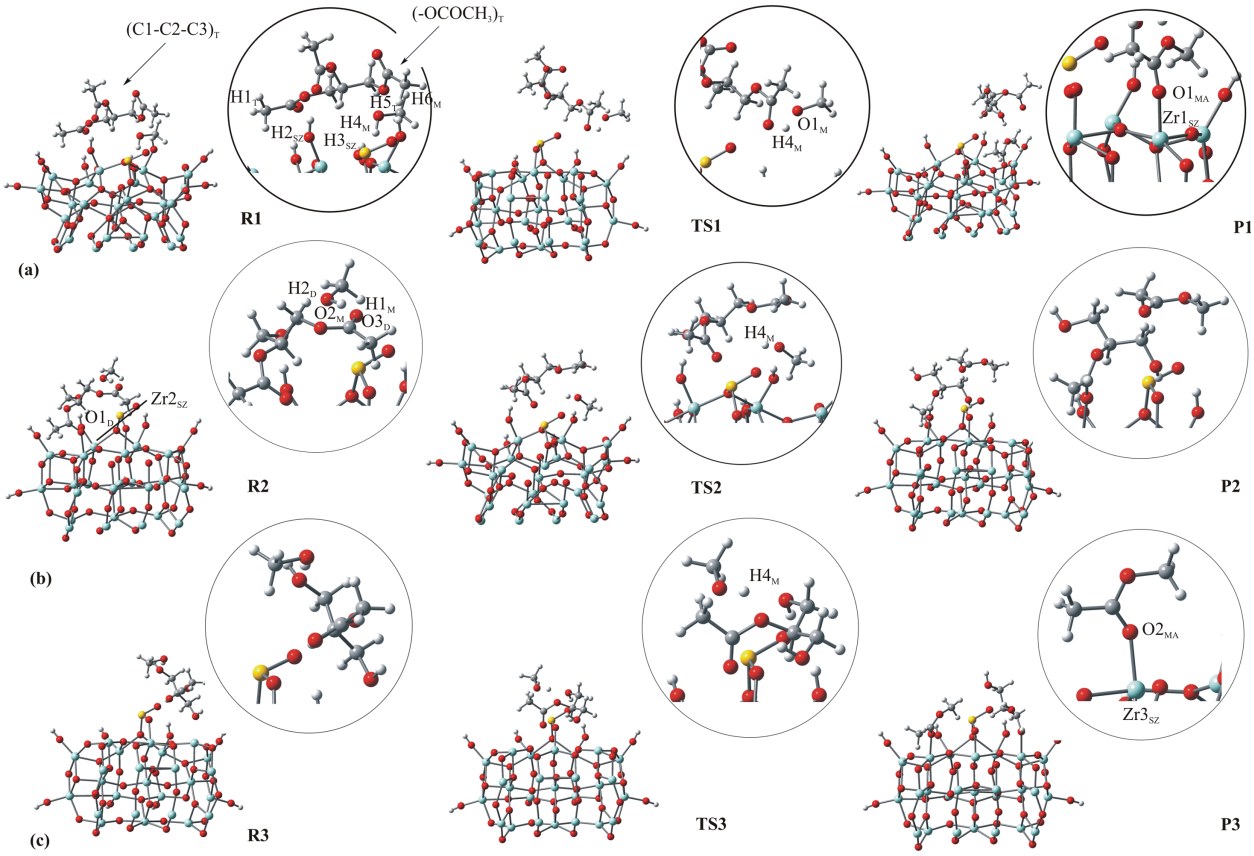

Figure 8. Close-ups of each of the reaction mechanisms reported in Figure 2: a) Structural representation of the reaction mechanism corresponding to **T** + **M** → **D** + **MA**. **R1** corresponds to the configuration of reactants. **TS1** corresponds to the transition-state configuration in step 1, and **P1** corresponds to geometrical orientation of the products. b) Structural representation of the reaction mechanism corresponding to **D** + **M** → **MO** + **MA**. **R2** corresponds to the configuration of reactants. **TS2** corresponds to the transition-state configuration in step 2, and **P2** corresponds to geometrical orientation of the products. c) Structural representation of the reaction mechanism corresponding to **MO** + **M** → **G** + **MA**. **R3** corresponds to the configuration of reactants. **TS3** corresponds to the transition-state configuration in step 3, and **P3** corresponds to geometrical orientation of the products. The subscripts denote where the atom or group belongs, that is, the subscript T is triacetin, D is diacetin, M is methanol, MA is methyl acetate, and SZ refers to the catalyst.

overall reaction. The Gibbs free energy, including zero-point energy corrections to account for contributions from the translational, rotational, and vibrational degrees of freedom, has been calculated. At this step, the Gibbs free energy is estimated to be $\Delta_r G_1^0 = -2.64$ kcal/mol, indicating that a favorable exergonic reaction may occur.

In the second step of the reaction, diacetin interacts with methanol in the presence of the SZ catalyst. A molecular representation of this configuration is presented in Figure 7b, and a close-up view is shown in Figure 8b. An adsorption energy of 58.0 kcal/mol was calculated for diacetin and methyl acetate (see Fig. 9). Diacetin is anchored to the SZ surface at a bonding distance of 222.4 pm via its $O1_D$ atom with the $Zr2_{SZ}$ atom at the SZ surface (see Fig. 8b). Methanol is tightly bound to diacetin. The interaction involves $O3_D$—$H1_M$ and $O2_M$—$H2_D$, with bond lengths of 161 and 177 pm, respectively (see close-up view at R2; Fig. 8b). This interaction distorts the geometry on the ZrO_2 surface with respect to that observed in the first step of the interaction; on average, the Zr—O bond distances are elongated by 3 pm. In contrast, the SO_3 structural parameters remain virtually unchanged. The interaction involving diacetin and methanol is significantly weakened at the transition state (TS2, in Fig. 8b) because the system undergoes a separation of 413 pm out of the SZ surface plane. This gives the organic system the opportunity to break the bonds on diacetin to allow transesterification to proceed. We calculate an activation energy of 24.2 kcal/mol and a Gibbs free energy of −5.71 kcal/mol for this process. This latter value corresponds

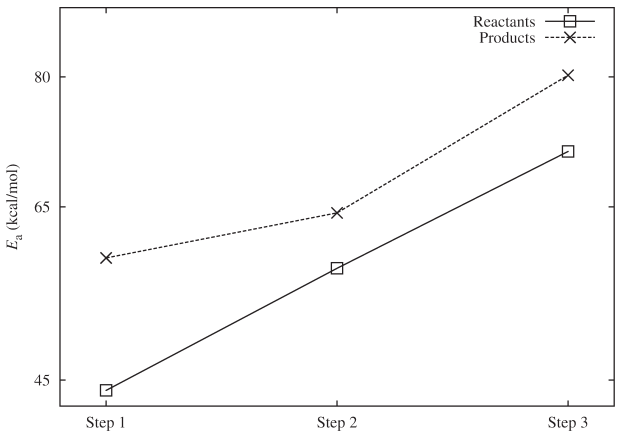

Figure 9. Adsorption energies (at the reactants and at the products) of the organic moieties attached to the SZ slab model in each of the three steps of the reaction mechanism.

to an exergonic reaction, which releases heat and may evolve with favorable thermodynamic conditions.

The optimized structure of the products is depicted in Figure 7b and P2 in Figure 8b. The resulting system at this step includes monoacetin and methyl acetate. Monoacetin is tightly bound to the SZ surface at the same Zr sites reported for the reactants. In this case, the attraction is stronger, with an interaction energy of 64.34 kcal/mol (see P2 in Fig. 8b) and a bonding distance from monoacetin to the SZ surface of 216 pm. We note that this configuration is 6 pm closer to the catalyst's surface than in the case of the reactants. This suggests an important role played by the Zr atoms at the surface. Such an interaction allows the formation of methyl acetate, which is weakly attached to monoacetin (at an average distance of 235 pm) and to the SZ catalyst (at a distance of 245 pm). Furthermore, methyl acetate interacts with one of the oxygen atoms of SO_3 (see P2 at Fig. 8b). Such an interaction may be identified as a short-range van der Waals-type attraction, which will be examined further in a future work. The slight structural changes observed for the catalyst's geometry are consistent with the experiment,[17] where the reactions occur only at sites located on or near the external surfaces of the solid catalysts, and where microporosity and any associated acidity would play a negligible role in the observed acidity of a catalyst.

Essentially, the third step of the overall reaction is governed by an analogous mechanism (see Fig. 7c and R3 at Fig. 8c). In this case, monoacetin is attached to the surface with a bond length of 223 pm and with an adsorption energy of 71.40 kcal/mol (see Fig. 9). The lattice is distorted because of the presence of the organic moiety. The transition state at this step behaves similar to that in the second step of the mechanism, and the organic moiety weakens the interaction with the surface, which is located 300 pm above it. The activation energy for this process is calculated to be 33 kcal/mol. This step concludes when monoacetin is transesterified to glycerol and a third molecule of methyl acetate (see Fig. 7c and P3 at Fig. 8c). Glycerol remains tightly bound to the SZ surface at an average bond distance of 221 pm, as shown at P3 in Figure 8c; here, the adsorption energy is 71.40 kcal/mol. Methyl acetate remains anchored to the surface at 220 pm from the closest Zr atom, as depicted at P3 ($O2_{MA}$—$Zr3_{SZ}$ bonding). The Gibbs free energy for this last process is $\Delta_r G_3^0 = -3.45$ kcal/mol (see Fig. 7c). Furthermore, the energy range of $\Delta_r G^0$ follows the following order: D → MA (S2) < MO → MA (S3) < T → MA (S1), where S1–S3 refer to the reaction steps 1 to 3, respectively, and T, D, MO, and MA correspond to triacetin, diacetin, monoacetin, and methyl acetate, respectively. In all the steps, $\Delta_r G^0$ is calculated to be negative, which may be directly assigned to exergonic reactions where no energy is required for the reaction to proceed, that is, all reactions in the three-step path are chemically favorable and have a high probability to progress. Additionally, the negative values for $\Delta_r G^0$ in steps 1 and 3 indicate favorable reactions, albeit slightly less favorable than those in step 2. This was verified by calculating the Gibbs free energies of activation ($\Delta^{\ddagger} G^0$) to gain insight into the rates of reaction for each step. This procedure gives $\Delta^{\ddagger} G^0(S3) = -129.83$ kcal/mol $< \Delta^{\ddagger} G^0(S2) = -105.86$ kcal/mol $< \Delta^{\ddagger} G^0(S1) = -94.44$ kcal/mol.

Table 2. Apparent activation energies from triacetin to diacetin conversion.

	Experimental (kcal/mol)	Theoretical (kcal/mol)
T → D (Heterogeneous)	12.0[a]	20.0[b]
T → D (Homogeneous)	11.0[a]	14.6[c]

[a] From Ref. 18. [b] From this work. [c] Averaged from Ref. 23.

It is important to note that the activation energy calculated for the first step of the reaction appears to be higher than that observed in the equivalent experimental work performed by López et al.[18] In that study, the apparent activation energy (E_{app}) for the conversion from triacetin to diacetin in the presence of Nafion® SAC-13[54] as the heterogeneous catalyst was found to be ~12 kcal/mol (see Table 2). This value was ~11 kcal/mol in the case of the homogeneously H_2SO_4 catalyzed reaction. The apparent activation energies are relevant if the fraction of the active sites of the catalyst occupied by the reactive molecules is small.[55] Because of the reduced number of particles used in the reaction coordinate of our model, the latter may also be assumed. The apparent activation energy[55] is given as the sum of the adsorption energy of the adsorbed reactant species and the activation energy (i.e., $E_{app} = E_{ac} + E_{ads}$).

Considering the results in Figure 9, the adsorption energy for the adsorbed triacetin on SZ corresponds to approximately −44 kcal/mol. (Note that the values in Fig. 9 are absolute quantities.) Given this value, the apparent activation energy E_{app} for the conversion of triacetin to diacetin in our calculations is ~20 kcal/mol (for comparison, see Table 2). Thus, we can assume that our theoretical results for the first step of the overall reaction are in reasonable agreement (with a difference of 8 kcal/mol) with the experiment.[18]

As noted previously, the activation energies for the second and third steps of the overall reaction are 24.2 and 33 kcal/mol, respectively. To the best of our knowledge, no analogous experimental data of apparent activation energies (E_{app}) for these steps have been reported. These values are higher than those determined for the first step reported previously.[18] This may be attributed to the lack of a predosed oxygen surface observed experimentally,[56] which refers to the presence of several O-atoms that may lower the reaction barrier. Another reason may be attributed to the defects on the surface, which may be present in the experiments and alter the results.[56] In our calculations, no defects on the SZ lattice were investigated. Another reason for this discrepancy may be strain, which has been observed in metal surfaces, such as Cu (111).[56] If the lattice parameter is allowed to relax, then the activation energy barrier is reduced by 1.4 kcal/mol. In our calculations, only the atoms closest to the surface area were allowed to relax. It is likely that if all parameters are considered in the optimization procedure, the barrier may be slightly reduced. Nevertheless, an examination of this assumption is

Table 3. Amount of charge donated and back-donated during the reaction mechanism in the three-step reaction.

	Donation (*e*)	Back-donation (*e*)
Step 1		
Reactants	−1.390	−0.054
Products	−1.022	−0.012
Step 2		
Reactants	−0.806	−0.045
Products	−0.927	−0.052
Step 3		
Reactants	−1.022	−0.114
Products	−0.942	−0.064

beyond the scope of the current study but will be considered in future work.

Charge donation and back-donation interactions

The intermolecular attraction described at the relaxed geometry of the reactants and products may also be understood from an analysis of charge donation interactions given by the CDA scheme (described in the "Computational Methods" section). The analysis is based on quantifying the electronic charge donated from the organic system (i.e., triacetin, its derivatives, and methanol) to the metallic surface and the back-donation from the metallic surface to the organic moiety. This description provides insight into the electronic energy in terms of the bonding of the organic moieties with the metallic surface. It is important to point out that CDA results can only give us a qualitative description of the tendencies involved in the donation/back-donation mechanism.[36] Nevertheless, no quantitative conclusions can be made as the aim of CDA methodology is only intended to give a qualitative picture of charge-transfer interactions. The approach specifically addresses the MOs that contribute to the interaction at the donation and back-donation schemes and computes the amount of charge transferred to the participating MOs from the organic systems, namely, the interactions of triacetin and methanol (T + M), diacetin and methyl acetate (D + MA), diacetin and methanol (D + M), monoacetin and methyl acetate (MO + MA), monoacetin and methanol (MO + M), and glycerol and methyl acetate (G + MA) to the SZ metal surface are examined. Additionally, this donation/back-donation interaction would only be important for the frontier molecular orbitals (HOMO) as their contributions as the acceptor and donor are the most likely sites where charge may be transferred. The CDA results in Table 3 are presented based on this assumption.

At the first step of the reaction coordinate, the charge donation arising from triacetin and methanol is −1.4 electrons (*e*). This corresponds to a contribution from the frontier MOs of the reactants, which are the highest energy orbitals that may play a role in this process. The back-donation contribution corresponds to −0.054*e*, that is, the adsorption at the catalyst is primarily ruled by a donation mechanism. The spatial representations of these MOs are depicted in Supporting Information Figure S1a.

The CDA results for the products show an analogous behavior, as the charge donation contribution has the same magnitude than in the reactants, that is, −1.0*e* are donated from the system formed by diacetin and methyl acetate to the SZ surface at the frontier MOs (see Supporting Information Fig. S1b), and only −0.012*e* are back-donated from the surface to the organic system, indicating that the charge donation is the driving force that gives rise to the adsorption of the organic system (diacetin and methyl acetate) on the metallic surface. The adsorption energy of the reactants in this configuration is 43.8 kcal/mol, whereas for the products is 59.1 kcal/mol (see Fig. 9).

The same tendency is followed in steps 2 and 3 of the reaction mechanism, where the charge donation interaction rules the bonding and the back-donation contribution from the HOMO represents in average, that is, only 7.2% of the average contribution coming from donation (see Table 3). In general, through all the reaction coordinates, back-donation contributing to the bonding may be considered negligible. On the other hand, the adsorption energies at the second step are 57.9 and 64.3 kcal/mol for the reactants and products, respectively. The largest adsorption energies are reported at step 3: 71.4 and 80.2 kcal/mol (see Fig. 9), corresponding to the reactants and products, respectively. Such energies are the largest along the trajectory and the bonding distances are the shortest among monoacetin–methyl acetate and the SZ surface, along the reaction coordinate. For the products at the third step, the bonding distance is also the shortest among all products in the reaction coordinate, strengthening the interaction. The frontier MOs involved in the electronic bonding energy at the reactants and products in steps 2 and 3 are also presented in Supporting Information Figure S1. Particularly, in the second step of the reaction coordinate, the donation contribution mainly resides at the hybridized sp and π*-orbitals of the Zr atoms at the HOMO. The back-donation transfer in this step may also be considered negligible as a small amount of charge goes from the SZ surface to the MOs at the MO + M system (see Table 3). Further contributions of the back-donated charge from the SZ surface are allocated at lower-energy hybridized sp orbitals on the O atoms of the MO + M system. An analogous behavior as that reported on the previous reaction steps is also present on the donation and back-donation mechanisms in the products of the third step. Donation rules the bonding as −1.0*e* resides on the frontier MOs of the SZ catalyst, whereas only −0.114*e* reside on the back-donated charge from frontier MOs at G + MA system as presented in Table 3.

To gain further insight into the molecular orbitals involved in each fragment (i.e., the SZ surface and the organic species), an energy decomposition analysis was performed at the ZORA level of theory using the optimized geometry of the reactants in the first step (see Fig. 10). It was found that the interaction involving triacetin–methanol and the SZ surface is primarily governed by the occupied MOs of the SZ fragment, which gives rise to the occupied MOs of the SZ-T + M system. In contrast, the triacetin–methanol fragment only participates with its highest MOs, which gives rise to the virtual MOs of the SZ-T + M system.

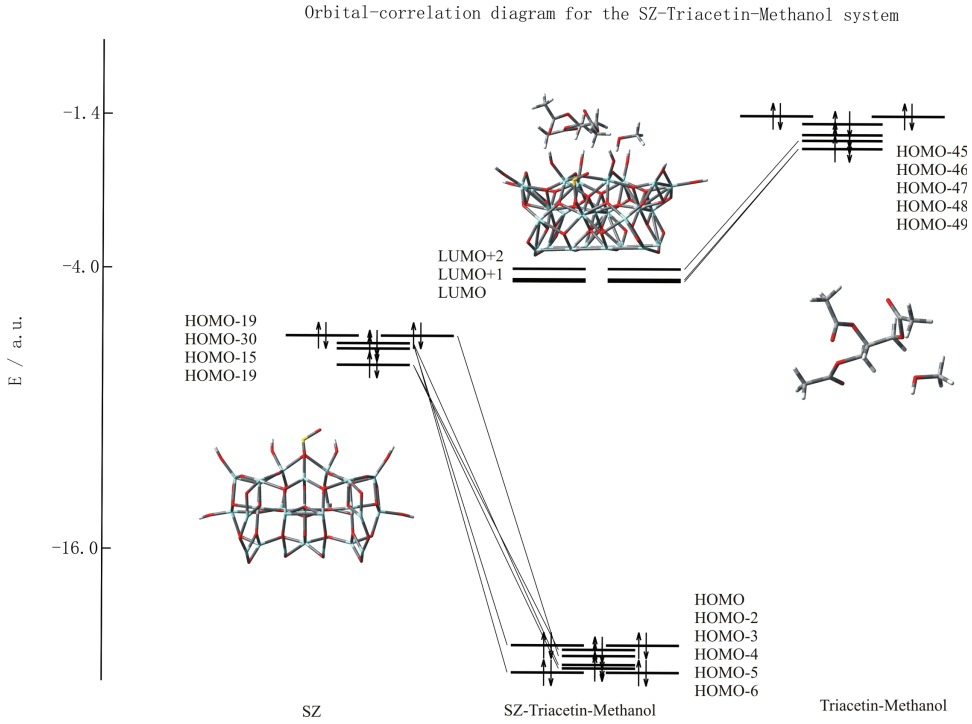

Figure 10. Orbital correlation diagram for the optimized reactants at step 1 in the reaction mechanism. Note that the SZ–triacetin–methanol system has been separated into an SZ fragment and a triacetin–methanol fragment. The corresponding MOs involved in the interaction are presented in the diagram. An analogous behavior may be found along the trajectory.

Conclusions

An ab initio study of the transesterification process involving a heterogeneous catalyst for biodiesel production was performed using an SZ cluster system to model the SZ acid catalyst. It was found that a strong acidity arises from an excess of positive charge located at the Zr atoms. A Fukui index analysis showed that the SZ model system is highly susceptible to catalytic activity, especially at the Zr sites with important contributions from the S atom. The three-step pathway of the transesterification process observed experimentally was modeled with the cluster catalyst, and three transition-state structures were found. Our results indicate that a charge donation mechanism is largely responsible for the bonding observed along the reaction coordinate. The Zr atoms initiate the transesterification reaction, with slight contributions from back-donation. The geometrical deformation of the SZ surface facilitates the adsorption of triacetin and other intermediates along the reaction coordinate. The acidic character of the Zr sites on the surface allows a strong adsorption of triacetin and the alcohol solvent. This causes an exchange of the H from the alcohol with a —COCH moiety of triacetin, which subsequently triggers the transesterification process to give the experimentally observed methyl acetate.

Acknowledgments

J.M. thanks Itzel Flores and Constanza Muñiz for technical support. J.M. also thanks Dirección General de Cómputo y de Tecnologías de Información y Comunicación (DGTIC) and the Supercomputing Department of the Universidad Nacional Autónoma de México for the computing resources under project No. SC15-1-IR-88. We also thank Dr. I.C. Romero-Ibarra for helpful discussion.

Keywords: biodiesel · density functional theory · heterogeneous catalysis · reaction mechanism · sulfated zirconia

How to cite this article: J. Muñiz, R. Castillo, B. Robles, E. Sansores. *Int. J. Quantum Chem.* **2016**, *116*, 988–999. DOI: 10.1002/qua.25116

[1] M. Zabeti, W. M. A. W. Daud, *Fuel Process. Technol.* **2009**, *90*, 770.
[2] A. K. Dalai, M. G. Kulkarni, L. C. Meher, *EEE EIC Climate Change Technology Conference EICCCC 2006*, **2006**, 4057358.
[3] S. Baroutian, M. K. Aroua, A. A. A. Raman, N. M. N. Sulaiman, *J. Chem. Eng. Data* **2008**, *53*, 877.
[4] H. Li, W. Xie, *J. Chem. Eng. Data* **2006**, *107*, 25.
[5] R. R. Tan, A. B. Culaba, M. R. I. Purvis, *Biomass Bioenergy* **2004**, *26*, 579.
[6] G. Arzamendi, E. Arguiñarena, I. Campo, S. Zabala, L. M. Gandía, *Catal. Today* **2008**, *133–135*, 305.
[7] G. Vicente, M. Martínez, J. Aracil, *Bioresour. Technol.* **2004**, *92*, 297.
[8] M. P. Dorado, E. Ballesteros, J. M. Arnal, J. Gómez, F. J. López, *Fuel* **2003**, *82*, 1311.
[9] M. P. Dorado, E. Ballesteros, J. A. Almeida, C. Schellert, H. P. Lohrlein, R. Krause, *Trans. ASAE* **2002**, *45*, 525.
[10] E. Lotero, Y. Liu, D. E. López, K. Suwannakarn, D. A. Bruce, J. G. Goodwin, *Ind. Eng. Chem.* **2005**, *44*, 5353.
[11] W. Du, Y. Y. Xu, D. H. Liu, J. Zeng, *J. Mol. Catal. B: Enzyme* **2004**, *30*, 125.
[12] A. Demirbas, *Energy Convers. Manage.* **2003**, *44*, 2093.
[13] S. Saka, D. Kusdiana, *Fuel* **2001**, *80*, 225.
[14] Y. Zhang, M. A. Dube, D. D. McLerean, M. Kates, *Bioresour. Technol.* **2003**, *89*, 1.
[15] X. Xiao, J. W. Tierney, I. Wender, *Appl. Catal. A: Gen.* **1999**, *183*, 209.
[16] M. Stocker, *J. Mol. Catal.* **1985**, *29*, 371.

[17] D. E. López, D. A. B. J. G. Goodwin, Jr., E. Lotero, *Appl. Catal. A: Gen.* **2005**, *295*, 97.
[18] D. E. López, K. Suwannakarn, D. A. Bruce, J. G. Goodwin, Jr., *J. Catal.* **2007**, *247*, 43.
[19] S. Ramu, N. Lingaiah, B. L. A. P. Devi, R. B. N. Prasad, I. Suryanarayana, P. S. S. Prasad, *Appl. Catal. A: Gen.* **2004**, *276*, 163.
[20] S. Furuta, H. Matsuhashi, K. Arata, *Catal. Commun.* **2004**, *5*, 721.
[21] H. A. Lara-García, I. C. Romero-Ibarra, H. Pfeiffer, *J. Solid State Chem.* **2014**, *218*, 213.
[22] N. Santiago-Torres, I. C. Romero-Ibarra, H. Pfeiffer, *Fuel Proc. Technol.* **2014**, *120*, 34.
[23] T. Limpanuparb, K. Punyain, Y. Tantirungrotechai, *J. Mol. Struct. (THEOCHEM)* **2010**, *955*, 23.
[24] N. C. O. Tapanes, D. A. G. Aranda, J. W. de Mesquita Carneiro, O. A. C. Antunes, *Fuel* **2008**, *87*, 2286.
[25] K. Hori, Y. Ikenaga, K. Arata, T. Takahashi, K. Kasai, Y. Noguchi, M. Sumimoto, H. Yamamoto, *Tetrahedron* **2007**, *63*, 1264.
[26] J. M. Fox, O. Dmitrenko, L. Liao, R. D. Bach, *J. Org. Chem.* **2004**, *69*, 7317.
[27] A. C. H. da Silva, C. A. Kuhnen, S. C. da Silva, E. L. Dall'Oglio, P. T. de Sousa, *Fuel* **2013**, *107*, 387.
[28] A. C. H. da Silva, E. L. Dall'Oglio, P. T. de Sousa, S. C. da Silva, C. A. Kuhnen, *Fuel* **2014**, *119*, 1.
[29] A. D. Becke, *J. Chem. Phys.* **1993**, *98*, 5648.
[30] C. Peng, H. B. Schlegel, *Israel J. Chem.* **1993**, *33*, 449.
[31] C. Peng, P. Y. Ayala, H. B. Schlegel, M. J. Frisch, *J. Comput. Chem.* **1996**, *17*, 49.
[32] K. A. Peterson, D. Figgen, M. Dolg, H. Stoll, *J. Chem. Phys.* **2007**, *126*, 124101.
[33] K. A. Peterson, B. C. Shepler, J. M. Singleton, *Mol. Phys.* **2007**, *105*, 445.
[34] G. A. Petersson, M. A. Al-Laham, *J. Chem. Phys.* **1991**, *94*, 6081.
[35] G. A. Petersson, A. Bennett, T. G. Tensfeldt, M. A. Al-Laham, W. A. Shirley, J. Mantzaris, *J. Chem. Phys.* **1988**, *89*, 2193.
[36] S. Dapprich, G. Frenking, *J. Phys. Chem.* **1995**, *99*, 9352.
[37] E. van Lenthe, E. J. Baerends, J. Snijders, *J. Chem. Phys.* **1993**, *99*, 4597.
[38] E. van Lenthe, E. J. Baerends, J. Snijders, *J. Chem. Phys.* **1994**, *101*, 9783.
[39] R. Parr, W. Yang, Density-Functional Theory of Atoms and Molecules; Oxford Science Publications: New York, **1989**.
[40] R. Parr, W. Yang, *J. Am. Chem. Soc.* **1984**, *106*, 4049.
[41] A. E. Reed, L. A. Curtiss, F. Weinhold, *Chem. Rev.* **1988**, *88*, 899.
[42] P. K. Chatarraj, B. Maiti, U. Sarkar, *J. Phys. Chem.* **2003**, *107*, 4973.
[43] M. J. Frisch, G. W. Trucks, H. B. Schlegel, G. E. Scuseria, M. A. Robb, J. R. Cheeseman, G. Scalmani, V. Barone, B. Mennucci, G. A. Petersson, H. Nakatsuji, M. Caricato, X. Li, H. P. Hratchian, A. F. Izmaylov, J. Bloino, G. Zheng, J. L. Sonnenberg, M. Hada, M. Ehara, K. Toyota, R. Fukuda, J. Hasegawa, M. Ishida, T. Nakajima, Y. Honda, O. Kitao, H. Nakai, T. Vreven, J. A. Montgomery, Jr., J. E. Peralta, F. Ogliaro, M. Bearpark, J. J. Heyd, E. Brothers, K. N. Kudin, V. N. Staroverov, R. Kobayashi, J. Normand, K. Raghavachari, A. Rendell, J. C. Burant, S. S. Iyengar, J. Tomasi, M. Cossi, N. Rega, J. M. Millam, M. Klene, J. E. Knox, J. B. Cross, V. Bakken, C. Adamo, J. Jaramillo, R. Gomperts, R. E. Stratmann, O. Yazyev, A. J. Austin, R. Cammi, C. Pomelli, J. W. Ochterski, R. L. Martin, K. Morokuma, V. G. Zakrzewski, G. A. Voth, P. Salvador, J. J. Dannenberg, S. Dapprich, A. D. Daniels, Ö Farkas, J. B. Foresman, J. V. Ortiz, J. Cioslowski, D. J. Fox, Gaussian 09, Revision B.01; Gaussian, Inc.: Wallingford, CT, **2009**.
[44] E. J. Baerends, J. Autschbach, A. Bérces, C. Bo, P. M. Boerrigter, L. Cavallo, D. P. Chong, L. Deng, R. M. Dickson, D. E. Ellis, L. Fan, T. H. Fischer, C. Fonseca-Guerra, S. J. A. van Gisbergen, J. A. Groeneveld, O. V. Gritsenko, M. Grüning, F. E. Harris, P. van den Hoek, H. Jacobsen, G. van Kessel, F. Kootstra, E. van Lenthe, V. P. Osinga, S. Patchkovskii, P. H. T. Philipsen, D. Post, C. C. Pye, W. Ravenek, P. Ros, P. R. T. Schipper, G. Schreckenbach, J. G. Snijders, M. Sola, M. Swart, D. Swerhone, G. te Velde, P. Vernooijs, L. Versluis, O. Visser, E. van Wezenbeek, G. Wiesenekker, S. K. Wolff, T. K. Woo, T. Ziegler, Amsterdam Density Functional (ADF), Theoretical Chemistry; Vrije Universiteit, Amsterdam. Available from: http://www.scm.com. Last accessed **2016**.
[45] C. Breitkopf, H. Papp, K. Li, R. Olindo, J. A. Lercher, R. Lloyd, S. Wrabetz, F. C. Jentoft, K. Meinel, S. Forster, K. M. Schindler, H. Neddermeyer, W. Widdra, A. Hofmann, J. Sauer, *Phys. Chem. Chem. Phys.* **2007**, *9*, 3600.
[46] X. Li, K. Nagaoka, L. J. Simon, R. Olindo, J. A. Lercher, A. Hoffman, J. Sauer, *J. Am. Chem. Soc.* **2005**, *127*, 16159.
[47] K. Meinel, A. Hofmann, S. F. Ana, R. Kulla, K. M. Schindler, H. Neddermeyer, J. Sauer, W. Widdra, *Phys. Chem. Chem. Phys.* **2005**, *8*, 1593.
[48] T. Kanougi, T. Atoguchi, S. Yao, *J. Mol. Catal. A: Chem.* **2002**, *177*, 289.
[49] A. Hofmann, J. Sauer, *J. Phys. Chem. B* **2004**, *108*, 14652.
[50] F. Gallino, C. D. Valentin, G. Pacchioni, *Phys. Chem. Chem. Phys.* **2011**, *13*, 17667.
[51] F. Babou, G. Coudurier, J. C. Vedrine, *J. Catal.* **1995**, *152*, 341.
[52] Z. Hong, K. B. Fogash, R. M. Watwe, B. Kim, B. I. Masqueda-Jiménez, M. A. Natal-Santiago, J. M. Hill, J. A. Dumesic, *J. Catal.* **1998**, *178*, 489.
[53] F. Haase, J. Sauer, *J. Am. Chem. Soc.* **1998**, *120*, 13503.
[54] M. A. Harmer, Q. Sun, A. J. Vega, W. E. Farneth, A. Heidekum, W. F. Hoelderich, *Green Chem.* **2000**, *2*, 7.
[55] R. Z. Khaliullin, A. T. Bell, *J. Phys. Chem. B* **2002**, *106*, 7832.
[56] J. Greeley, M. Mavrikakis, *J. Catal.* **2002**, *208*, 291.

Received: 30 October 2015
Revised: 13 January 2016
Accepted: 4 February 2016
Published online 27 February 2016